scale factor for NH ob and CN t might be different from that for CO ob; additional experimental data will be needed to test this point. We note that this scale factor cannot be fixed by an assignment of the observed 633-cm^{-1} band to the CO ob mode now calculated at 607 cm^{-1}; the latter contains NH ob, and our experimental results indicate that the 633-cm^{-1} band is unshifted in D_2O, confirming its assignment to the CO ib mode.

For *c*-NMA (Table VI), analogous changes are seen, although we can be less certain about details because of the paucity of data, which led us to maintain the scale factors of the isolated molecule. These nevertheless reproduce quite well the amide II like mode observed at 1496 cm^{-1} [22,23] and show that there is a significant change in its character on hydrogen bonding. The amide I mode interacts strongly with HOH bend, a result of the near-coincidence in frequencies for the current value of the CO s scale factor; additional data will be needed to verify this prediction. Amide III is predicted to increase (from 1331 to 1354 cm^{-1}), but this band has not been observed. The presence of a *cis* band at 821 cm^{-1}, well separated from the similar *trans* band at 886 cm^{-1}, is clearly seen[23] and is reasonably well reproduced by the calculation.

Conclusions

In order to examine the effect that hydrogen bonding has on the frequencies and normal modes of NMA, we have compared the *ab initio* force constants, frequencies, and modes of isolated *t*-NMA and *c*-NMA with those of a model system in which the NH and CO groups are each hydrogen bonded to a water molecule. While such an NMA-$(H_2O)_2$ model cannot realistically represent the water structure surrounding the NMA molecule in aqueous solution, it should provide an appropriate description of the characteristic changes that hydrogen bonding produces in the vibrational dynamics of the NMA molecule.

For *t*-NMA-$(H_2O)_2$, calculations at the 4-31G* level (which provided satisfactory scaled force constants and vibrational modes for the isolated molecule[6]) together with readily assigned observed bands led to optimized scale factors that resulted in good agreement between observed and calculated frequencies (the average discrepancy for observed bands below 1700 cm^{-1} is 5.1 cm^{-1}). The expected increases in bond lengths on hydrogen bonding are found for the NH and CO bonds. The accompanying shortening of the CN bond indicates that its double-bond character increases on hydrogen bonding. Associated changes in force constants correlate well with these geometric changes and with other expected effects of hydrogen bonding.

The calculated *c*-NMA-$(H_2O)_2$ results are more difficult to scale because of the limited experimental data on this molecule in aqueous solution. Transfer of scale factors without change from the isolated molecule[7] could nevertheless confirm the assignments of a new band at 1496 cm^{-1} in high-energy-pulsed resonance Raman spectra to the amide II like mode of *c*-NMA[22,23] and a new band at 821 cm^{-1} to this isomer as well.[23] While trends in force constant changes on hydrogen bonding are generally similar to those in *t*-NMA, more reliable values will have to await optimization of scale factors based on more extensive data.

Acknowledgment. This research was supported by National Science Foundation Grants DMB-8816756 and DMR-8806975.

Supplementary Material Available: Table giving scaled off-diagonal force constants of hydrogen-bonded *t*-NMA and *c*-NMA (3 pages). Ordering information is given on any current masthead page.

Vibrational Circular Dichroism and Absolute Configuration of Substituted Thiiranes

Prasad L. Polavarapu,*,† Simeon T. Pickard,† Howard E. Smith,*,† Thomas M. Black,† Arvi Rauk,*,‡ and Danya Yang‡

Contribution from the Departments of Chemistry, Vanderbilt University, Nashville, Tennessee 37235, and University of Calgary, Calgary, Alberta, Canada T2N 1N4.
Received April 22, 1991

Abstract: Experimental vibrational circular dichroism (VCD) spectra for *trans*-2,3-dimethylthiirane and its *2,3-d_2* isotopomer were measured in the 1600-700-cm^{-1} region. Ab initio theoretical calculations of VCD using the localized molecular orbital formalism were carried out with the 6-31G* basis set. Similar calculations were also done using the vibronic coupling formalism for *trans*-2,3-dimethylthiirane, its *2,3-d_2* isotopomer, and methylthiirane. A comparison between the theoretical model predictions and the experimental data reveals that the theoretical models are successful in reproducing the experimental VCD spectra. The merits and limitations of the individual models are discussed.

Introduction

Vibrational circular dichroism (VCD) is anticipated to provide new approaches to the determination of three-dimensional structure of chiral molecules in isotropic media. Experimental techniques[1-6] have developed to the extent that reliable spectra can be obtained anywhere from the near-infrared region to the long-wavelength side of the mid-infrared region (~700 cm^{-1}). At the same time, three different quantum-theoretical methods became available[7-15] for predicting the VCD spectra. One of the current active research areas involves testing these theoretical methods for their predictive capability. Small chiral molecules which can be subjected to a rigorous theoretical vibrational analysis are crucial for this purpose. For this reason, recent theoretical evaluations were focused on 2,3-dideuteriooxirane,[15-17] 1,2-di-

† Vanderbilt University.
‡ University of Calgary.

(1) (a) Holzwarth, G.; Hsu, E. C.; Mosher, H. S.; Faulkner, T. R.; Moscowitz, A. *J. Am. Chem. Soc.* **1974**, *96*, 251-252. (b) Nafie, L. A.; Keiderling, T. A.; Stephens, P. J. *J. Am. Chem. Soc.* **1976**, *98*, 2715-2723.
(2) Cianciosi, S. J.; Ragunathan, N.; Freedman, T. B.; Nafie, L. A.; Baldwin, J. E. *J. Am. Chem. Soc.* **1990**, *112*, 8204-8206.
(3) Narayanan, U.; Keiderling, T. A.; Elsevier, C. J.; Vermeer, P.; Runge, W. *J. Am. Chem. Soc.* **1988**, *110*, 4133-4138.
(4) Diem, M.; Roberts, G. M.; Lee, O.; Barlow, A. *Appl. Spectrosc.* **1988**, *42*, 20-26.
(5) For a collection of references on the subject, see: Polavarapu, P. L. In *Vibrational Spectra and Structure*, Bist, H. D., Durig, J. R., Sullivan, J. F., Eds.; Elsevier: New York, 1989; Vol. 17B, pp 319-342.
(6) Polavarapu, P. L. *Appl. Spectrosc.* **1989**, *43*, 1295-1297.
(7) Walnut, T. W.; Nafie, L. A. *J. Chem. Phys.* **1977**, *67*, 1501-1510.
(8) Nafie, L. A.; Walnut, T. W. *Chem. Phys. Lett.* **1977**, *49*, 441-446.

0002-7863/91/1513-9747$02.50/0

deuteriocyclopropane,[18,19] methyloxirane,[20,21] 2,3-dimethyloxirane,[21] ethanol-α-d,[22] and methylthiirane.[23-25] Qualitatively correct theoretical predictions were obtained for these molecules, but detailed quantitive evaluations are yet to be undertaken in most cases.

In the localized molecular orbital (LMO) method,[7-9] the expression of rotational strength for a vibrational normal mode j is given as

$$R_j = \frac{e^2\hbar}{4c}[\{\sum_{n=1}^{n_{nuclei}}\xi_n\mathbf{S}_n^j - \sum_{i=1}^{n_{electrons}}\sigma_i^j\}\cdot\{\sum_{n=1}^{n_{nuclei}}\xi_n(\mathbf{R}_n\times\mathbf{S}_n^j) - \sum_{i=1}^{n_{electrons}}\mathbf{r}_i^0\times\sigma_i^j\}] \quad (1)$$

where ξ_n is the bare nuclear charge of atom n with positional vector $\mathbf{R}_n$ and displacement vector $\mathbf{S}_n^j = (\partial\mathbf{R}_n/\partial Q_j)$ during a normal vibrational mode Q_j, $\mathbf{r}_i^0$ is the centroid of the localized molecular orbital occupied by the ith electron, and $\sigma_i^j = (\partial\mathbf{r}_j/\partial Q_j)$ is the displacement of the orbital centroid during vibration j.

In the vibronic coupling theoretical (VCT)[14] method, the individual electric and magnetic dipole transition moments become respectively

$$\mu^{vc}_{(00,01)j} = e\left(\frac{\hbar}{2\omega_j}\right)^{1/2}\left[\sum_{n=1}^{n_{atoms}}\xi_n\mathbf{S}_n^j - 2\sum_{n=1}^{n_{atoms}}\sum_{i=1}^{n_{electrons}}\sum_{e=1}^{n_{ex}}\langle\Psi_0|\mathbf{r}_i|\Psi_e\rangle\left\langle\Psi_e\left|\frac{\partial}{\partial\mathbf{R}_n}\right|\Psi_0\right\rangle\mathbf{S}_n^j\right] \quad (2.1)$$

$$= e\left(\frac{\hbar}{2\omega_j}\right)^{1/2}\left[\sum_{n=1}^{n_{atoms}}\xi_n\mathbf{S}_n^j - 2\sum_{n=1}^{n_{atoms}}\sum_{i=1}^{n_{electrons}}\left\langle\Psi_0|\mathbf{r}_i\frac{\partial}{\partial\mathbf{R}_n}\right|\Psi_0\right\rangle\mathbf{S}_n^j\right] \quad (2.2)$$

and

$$\mathbf{m}^{vc}_{(00,01)j} = \frac{e}{2c}\left(\frac{\hbar\omega_j}{2}\right)^{1/2}\left[i\sum_{n=1}^{n_{atoms}}\xi_n(\partial\mathbf{R}_n\times\mathbf{S}_n^j) - 2\sum_{n=1}^{n_{atoms}}\sum_{i=1}^{n_{electrons}}\sum_{e=1}^{n_{ex}}\langle\Psi_0|\mathbf{r}_i\times\mathbf{p}_i|\Psi_e\rangle\left\langle\Psi_e\left|\frac{\partial}{\partial\mathbf{R}_n}\right|\Psi_0\right\rangle\mathbf{S}_n^j\frac{1}{E_e^0 - E_0^0}\right] \quad (3)$$

where $\mathbf{r}_i$ and $\mathbf{p}_i$ are the position and momentum of the ith electron, ω_j is the frequency of the jth normal mode, and $E_e^0 - E_0^0$ is the vertical electronic excitation energy. The electronic wave functions are denoted Ψ_0 and Ψ_e. The energy difference and all matrix elements are evaluated at the equilibrium geometry of the ground state. The superscript vc denotes that these expressions describe a vibronic coupling mechanism for IR and VCD intensities. The subscript (00,01) signifies that the transition is between the v = 0 and v = 1 vibrational levels of the ground electronic state of the molecule. The VCT rotational strength is the imaginary part of the scalar product of $\mu^{vc}_{(00,01)j}$ and $\mathbf{m}^{vc}_{(00,01)j}$.

In this paper, we present the experimental VCD data for *trans*-2,3-dimethylthiirane and *trans*-2,3-dimethylthiirane-*2,3-d*$_2$, in the 1600–700-cm^{-1} region. The ab initio calculations of VCD using the LMO[7] and VCT[14] formalisms are also presented and quantitatively compared. VCT calculations are also presented for 2-methylthiirane and compared to the previously reported LMO and magnetic field perturbative (MFP) model predictions[23-25] and to the experimental data.[25]

Table I. Physical Data for Thiiranes

compound	bp, °C	α^{23-25}_D(neat, 0.5 dm)	% ee
(±)-2,3-dimethylthiirane	80–84		
(2*R*,3*R*)-2,3-dimethylthiirane[a]	80–84	+46.4	81
(2*R*,3*R*)-2,3-dimethylthiirane-*2,3-d*$_2$	80–84	+43.3	76[c]
(2*S*,3*S*)-2,3-dimethylthiirane-*2,3-d*$_2$	80–84	−42.5	75[c]
(*R*)-methylthiirane[b]	73–74	+22.8	94
(*S*)-methylthiirane[b]	73–74	−19.5	81

[a] d^{25}_4 0.8863. [b] d^{18}_4 0.946. [c] Estimated uncertainty ±5%.

Experimental and Computational Details

The thiiranes (Table I) were prepared by the reaction of the corresponding oxirane with potassium thiocyanate in water.[25b,26] (2*S*,3*S*)-2,3-Dimethylthiirane was characterized earlier,[27] and the percentage enantiomeric excess (% ee) of the 2*R*,3*R* isomer shown in Table I is based on the highest rotatory power previously reported[27] for the 2*S*,3*S* isomer. The enantioenrichment for (2*R*,3*R*)- and (2*S*,3*S*)-2,3-dimethylthiirane-d_2 is based on the optical purity of the corresponding oxiranes from which these thiiranes were prepared and on the assumption that the conversion to the thiirane proceeds with complete inversion of configuration.[26] The oxiranes used in these preparations, (2*S*,3*S*)- and (2*R*,3*R*)-2,3-dimethyloxirane-d_2 (α^{23}_D − 18.3° (neat, 0.5 dm) and α^{23}_D + 18.1° (neat, 0.5 dm), respectively), will be described elsewhere,[28] their respective enantioenrichments being determined using the chiral ^{1}H NMR shift reagent[29] tris[3-((trifluoromethyl)hydroxymethylene)-(+)camphorato]-europium(III) (Eu(tfc)$_3$) in benzene-d_6 with the 2*R*,3*R* isomer. For (*R*)- and (*S*)-methylthiirane, the respective % ee's are based on the maximum rotatory power reported[30] for the *S* isomer.

Each thiirane was shown on the basis of its ^{1}H NMR spectrum in chloroform-*d* with tetramethylsilane (TMS) as the internal standard to be free of impurities. (±)- and (2*R*,3*R*)-2,3-dimethylthiirane showed proton signals downfield from TMS at 1.49 (d, 6 H, J = 5.4 Hz, CH$_3$) and 2.64 ppm (m, 2 H, CH), while (2*R*,3*R*)- and (2*S*,3*S*)-2,3-dimethylthiirane-d_2, as expected, showed only one proton signal at 1.48 ppm (s, CH$_3$). (*R*)- and (*S*)-methylthiirane have spectra identical to that reported earlier[25b] for the *R* isomer.

VCD spectra in the 1600–700-cm^{-1} region were measured, at 4-cm^{-1} resolution, on a VCD instrument[6] built at Vanderbilt. A liquid-nitrogen-cooled HgCdTe detector (D^* = 4 × 10^{10}, 600-cm^{-1} cutoff), ZnSe photoelastic modulator, and KRS-5 polarizer were used for the spectra presented here. The baseline artifacts were minimized by subtracting the raw VCD of the racemic mixture from that of the (+)-enantiomer or by taking half of the difference between the raw VCD of the (+) and (−) enantiomers. The experimental rotational strengths, R, were determined from the frequency weighted integrated areas as[31]

$$R = \frac{0.23\times10^{-38}}{cl}\int\frac{\Delta A(\nu)}{\nu}\,d\nu \approx \frac{0.23\times10^{-38}}{cl\nu_0}\int\Delta A(\nu)\,d\nu \quad (4)$$

where c is the concentration, l is the path length, ν_0 is the band center, and $\Delta A(\nu) = A_L(\nu) - A_R(\nu)$ with $A_L(\nu)$ and $A_R(\nu)$ representing respectively the absorbance for left and right circularly polarized light at frequency ν. The observed rotational strengths are corrected for enantiomeric excess so that the tabulated values correspond to the pure enantiomers. The experimental vibrational intensities were determined in two

(9) Nafie, L. A.; Polavarapu, P. L. *J. Chem. Phys.* **1981**, *75*, 2935–2944.
(10) Galwas, P. A. *Ph.D. Thesis*, Cambridge University, Cambridge, U.K., 1983.
(11) Buckingham, A. D.; Fowler, P. W.; Galwas, P. A. *Chem. Phys.* **1987**, *112*, 1–14.
(12) Stephens, P. J. *J. Chem. Phys.* **1985**, *89*, 748–752.
(13) Morokuma, K. J.; Sugeta, H. *Chem. Phys. Lett.* **1987**, *134*, 23–26.
(14) Nafie, L. A.; Freedman, T. B. *J. Chem. Phys.* **1983**, *78*, 7106–7108.
(15) (a) Dutler, R. *Ph.D. Dissertation*, University of Calgary, Calgary, AB, Canada, 1988. (b) Dutler, R.; Rauk, A. *J. Am. Chem. Soc.* **1989**, *111*, 6957–6966.
(16) Stephens, P. J.; Jalkanen, K. J.; Kawiecki, R. W. *J. Am. Chem. Soc.* **1990**, *112*, 6518–6529.
(17) Polavarapu, P. L.; Bose, P. K. *J. Chem. Phys.* **1990**, *93*, 7524–7525.
(18) Jalkanen, K. J.; Kawiecki, R. W.; Stephens, P. J.; Amos, R. D. *J. Phys. Chem.* **1990**, *94*, 7040–7055.
(19) Polavarapu, P. L.; Bose, P. K. *J. Phys. Chem.* **1991**, *95*, 1606–1608.
(20) Kawiecki, R. W.; Devlin, F.; Stephens, P. J.; Amos, R. D.; Handy, N. C. *Chem. Phys. Lett.* **1988**, *145*, 411–417.
(21) Rauk, A.; Yang, D. *J. Am. Chem. Soc.*, in press.
(22) Shaw, R. A.; Wieser, H.; Dutler, R.; Rauk, A. *J. Am. Chem. Soc.* **1990**, *112*, 5401–5410.
(23) Dothe, H.; Lowe, M. A.; Alper, J. S. *J. Phys. Chem.* **1988**, *92*, 6246–6249.
(24) Amos, R. D.; Handy, N. C.; Palmieri, P. *J. Chem. Phys.* **1990**, *93*, 5796–5804.
(25) (a) Polavarapu, P. L.; Bose, P. K.; Pickard, S. T. *J. Am. Chem. Soc.* **1991**, *113*, 43–48. (b) Polavarapu, P. L.; Hess, B. A., Jr.; Schaad, L. J.; Henderson, D. O.; Fontana, L. P.; Smith, H. E.; Nafie, L. A.; Freedman, T. B.; Zuk, W. M. *J. Chem. Phys.* **1987**, *86*, 1140–1146.
(26) Snyder, H. R.; Stewart, J. M.; Ziegler, J. B. *J. Am. Chem. Soc.* **1947**, *69*, 2672–2674.
(27) Helmkamp, G. K.; Schnautz, N. *Tetrahedron* **1958**, *2*, 304–307.
(28) Pickard, S. T.; Polavarapu, P. L.; Smith, H. E. To be published.
(29) McCreary, M. D.; Lewis, D. W.; Wernick, D. L.; Whitesides, G. M. *J. Am. Chem. Soc.* **1974**, *96*, 1038–1054.
(30) Tsunetsugu, T.; Furukawa, J.; Fueno, T. *J. Polym. Sci., Polym. Chem. Ed.* **1971**, *9*, 3541–3546.
(31) Faulkner, T. R. *Ph.D. Thesis*, University of Minnesota, 1976.

Table II. 6-31G* and 6-31G*$^{(0.3)}$ Geometries of Thiirane, 2-Methylthiirane, and *trans*-2,3-Dimethylthiirane

	thiirane (C_{2v})			2-methylthiirane (C_1)		*trans*-2,3-dimethylthiirane (C_2)	
param[a]	6-31G*	6-31G*$^{(0.3)}$	exptl[b]	6-31G*	6-31G*$^{(0.3)}$	6-31G*	6-31G*$^{(0.3)}$
a	1.473	1.482	1.484 (1.492)	1.472	1.481	1.472	1.481
b	1.075	1.079	1.083 (1.078)	1.075	1.080	1.511	1.516
c	1.075	1.079	1.083 (1.078)	1.511	1.516	1.511	1.516
d	1.075	1.079	1.083 (1.078)	1.076	1.080	1.078	1.082
e	1.075	1.079	1.083 (1.078)	1.077	1.081	1.078	1.082
f	1.811	1.829	1.815 (1.819)	1.822	1.840	1.824	1.842
g	1.811	1.829	1.815 (1.819)	1.814	1.832	1.824	1.842
h				1.084	1.089	1.084	1.089
i				1.087	1.092	1.087	1.093
j				1.083	1.089	1.083	1.088
ab	118.3	118.3		118.8	118.7	121.2	121.7
ac	118.3	118.3		120.7	121.2	121.2	121.7
ad	118.3	118.3		118.0	118.0	115.3	115.0
ae	118.3	118.3		115.6	115.3	115.3	115.0
af	66.0	66.1	65.9 (65.8)	65.9	65.9	66.2	66.3
ag	66.0	66.1	65.9 (65.8)	66.4	66.5	66.2	66.3
bd	114.8	115.2	115.8 (116.0)	114.6	115.1	114.4	114.8
bg	115.3	114.9		115.2	114.9	118.8	118.5
ce	114.6	115.2		114.6	115.0	114.4	114.8
cf	115.3	114.9		118.9	118.7	118.8	118.5
ch				110.9	110.9	110.9	110.8
ci				111.0	109.9	109.9	110.0
cj				111.0	110.9	111.0	110.9
dg				115.0	114.7	112.2	111.5
ef				112.4	111.6	112.2	111.5
hi				108.2	108.2	108.1	108.2
hj				108.2	108.3	108.2	108.3
ij				108.6	108.6	108.6	108.6
bac	−146.1	−147.0		−142.7	−143.2	−139.3	−140.0
bae	0.0	0.0		2.5	3.0	5.9	6.2
baf	106.9	106.5		106.9	106.6	110.4	110.0
cag	106.9	106.5		110.4	110.1	110.4	110.0
dae	146.1	147.0		148.7	149.9	151.1	152.5
daf	−106.9	−106.5		−106.9	−106.5	−104.4	−103.7
eag	−106.9	−106.5		−104.4	−103.6	−104.4	−103.7
ach				−155.7	−155.7	−155.9	−155.1
aci				84.8	84.8	84.6	85.4
acj				−35.3	−35.3	−35.6	−34.8

[a] See Figure 1 for a definition of the parameters. The letters denote bonds; e.g. a is the length (Å), ab is the bond angle (deg), and abc is the dihedral angle (deg). [b] The r_s geometry;[42a] numbers in parentheses are the r_0 geometry.[42b]

ways: by fitting of Lorentzian curves to the experimental IR spectrum in CCl_4 after subtracting the solvent absorptions; from the integrated areas as

$$A = \frac{1}{cl}\int \ln \frac{I_0}{I}\, d\nu = \frac{2.303}{cl}\int \log \frac{I_0}{I}\, d\nu \qquad (5)$$

In cases where two or more bands overlap, the combined integrated band intensities are presented. The band overlap is not as much of a problem for rotational strengths as it is for absorption intensities, since VCD, being 4 orders of magnitude smaller, approaches the zero line much sooner than the corresponding absorption. The absorption intensities of individual bands determined by a curve-fitting procedure (after the solvent absorption was subtracted) are approximate due to some arbitrariness in the curve-fitting procedure itself and vary for the spectra obtained in different solvents by small but significant amounts. Similarly, the experimental frequencies depend on whether the spectra were taken for neat liquid or for solutions and on the nature of the solvent. For simplicity, only the frequencies for neat liquids are listed.

The geometries of *trans*-dimethylthiirane and methylthiirane were determined by complete optimization at the restricted Hartree–Fock level of theory using the analytical procedures of the GAUSSIAN 82[32] or GAUSSIAN 86[33] system of programs and the internal 6-31G* basis set and the modified 6-31G*$^{(0.3)}$ basis set.[21,34] Normal-mode coordinate analyses at 6-31G**,[35] 6-31G*, and 6-31G*$^{(0.3)}$ [34] equilibrium geometries were carried out by analytical second differentiation of the Born–Oppenheimer RHF energy[36] with the CADPAC[37] or GAUSSIAN 86 programs. For LMO–IR and LMO–VCD intensities, the localized orbital centroids were obtained through Boys' localization scheme[38] as implemented in the GAMESS program.[39] The derivatives of orbital centroids were obtained numerically by displacing the nuclei by 0.005 Å. The VCT–IR and VCT–VCD intensities were accomplished by the program system FREQ86,[40] which implements the vibronic coupling theory of Nafie and Freedman[14] at the ab initio level. The absorption intensities obtained in the LMO calculation should be identical to the corresponding values in the analytical

(32) (a) Binkley, J. S.; Frisch, M. J.; Defrees, D. J.; Raghavachari, K.; Whitesides, R. A.; Schlegel, H. B.; Fluder, E. M.; Pople, J. A. *GAUSSIAN 82*; Carnegie-Mellon University: Pittsburgh, PA, 1982. (b) Rauk, A.; Dutler, R. *J. Comput. Chem.* **1987**, *8*, 324.

(33) Frisch, M. J.; Binkley, J. S.; Schlegel, H. B.; Raghavachari, K.; Melius, C. F.; Martin, L. R.; Stewart, J. J. P.; Bobrowicz, F. W.; Rohlfing, C. M.; Kahn, L. R.; De Frees, D. J.; Seeger, R.; Whiteside, R. A.; Fox, D. J.; Fleuder, E. M.; Pople, J. A. *GAUSSIAN 86*; Carnegie-Mellon Publishing Unit: Pittsburgh, PA, 1986. The version at the University of Calgary was modified to write Fock and overlap matrix derivatives to the read-write file for VCD calculations.

(34) The 6-31G*$^{(0.3)}$ basis set is derived from the conventional 6-31G* basis set by changing the d exponent of C, N, and O from 0.8 to 0.3. Recent studies by Rauk and Yang have revealed that this basis set yields VCT–VCD results which are in good agreement with experimental measurements in the mid-infrared region of the spectrum for a series of molecules containing first-row atoms.[21] In addition, bond lengths are calculated to be longer than and closer to experimental values than with the 6-31G* basis set.[21] Tests (unpublished) on small sulfur-containing systems suggest that it is unnecessary to alter the d exponent (0.65) for the S atom.

(35) Hariharan, P. C.; Pople, J. A. *Chem. Phys. Lett.* **1972**, *66*, 217.

(36) Pulay, P. In *Methods of Electronic Structure Theory*; Schaefer, H. F., III, Ed.; Modern Theoretical Chemistry, Vol. 3; Plenum: New York, 1977.

(37) Amos, R. D.; Rice, J. E. *CADPAC: The* Cambridge *Analytical Derivatives Package, Version 4*; Cambridge University: Cambridge, U.K., 1987.

(38) Foster, J. M.; Boys, S. F. *Rev. Mod. Phys.* **1960**, *32*, 300–302.

(39) (a) Schmidt, M. W.; Boatz, J. A.; Baldridge, K. K.; Koseki, S.; Gordon, M. S.; Eldbert, S. T.; Lam, B. *QCPE Bull.* **1987**, *7*, 115. (b) Dupuis, M.; Spangler, D.; Wendoloski, J. J. *NRCC Program QG01*; University of California: Berkeley, CA, 1980.

(40) FREQ86: a version of FREQ85[15] modified to be compatible with GAUSSIAN 86.[33]

Table III. Vibrational Frequencies of *trans*-2,3-Dimethylthiirane and *trans*-2,3-Dimethylthiirane-*2,3-d*$_2$

		trans-2,3-dimethylthiirane					*trans*-2,3-dimethylthiirane-*2,3-d*$_2$			
		freq, cm^{-1}					freq, cm^{-1}			
no.	sym	calc[b]	calc[c]	calc[d]	exptl	assignt[a]	sym	calc[a]	calc[d]	exptl	assignt[a]
9	a	1641	1626	1625	1458	CH_3 def	a	1639	1623	1452	CH_3 def
10	b	1640	1624	1624		CH_3 def	b	1638	1623		CH_3 def
11	a	1633	1617	1617	1444	CH_3 def	a	1631	1615	1439	CH_3 def
12	b	1629	1612	1613		CH_3 def	b	1629	1612		CH_3 def
13	a	1592	1582	1568	1394	∥CH + CH_3 def	a	1568	1532	1375	CH_3 umb
14	b	1566	1552	1528	1376	CH_3 umb	b	1564	1562		CH_3 umb
15	a	1559	1544	1522		CH_3 umb	a	1491	1478	1323	ring CC str + CH_3 umb
16	b	1462	1452	1434	1295	∥CH	b	1268	1250	1129	CH_3 rock + ∥CD
17	a	1307	1301	1294	1196	ring CC str + ∥CH	a	1242	1227	1115	CH_3 rock
18	a	1290	1284	1273	1154	⊥CH + CH_3 rock	b	1191	1175	1065	CH_3 rock + C–CH_3 str
19	b	1233	1226	1210	1088	⊥CH + CH_3 rock	a	1184	1167	1053	CH_3 rock
20	a	1189	1183	1172	1057[e]	⊥CH + CH_3 rock	b	1147	1132	1032	CCH_3 str + CH_3 rock
21	b	1179	1173	1164	1066[e]	CCH_3 str + CH_3 rock	a	1009	995	913	∥CD +
22	a	1102	1095	1083	989[e]	⊥CH + CH_3 rock	b	917	902	835	∥CD + CH_3 rock
23	b	1092	1087	1079	978[e]	CCH_3 str + CH_3 rock	a	871	858	802	CCH_3 str + ring CC str
24	b	1066	1060	1049	950	⊥CH + CH_3 rock	b	862	842	757	⊥CD + CH_3 rock
25	a	900	897	887	834	ring CC str + C–CH_3 str	a	851	832	757	⊥CD

[a] From computer animation of normal modes. Terminology: ⊥ = perpendicular to ce or bd plane (Figure 1), ∥ = parallel to ce or bd, str = stretch, def = deformation, umb = umbrella motion. [b] 6-31G*, unscaled. [c] 6-31G**, unscaled. [d] 6-31G*$^{(0.3)}$, unscaled. [e] See text for a discussion.

Table IV. Experimental and Theoretical Vibrational Properties for *trans*-2,3-Dimethylthiirane in the 1600–700-cm^{-1} Region

frequencies, cm^{-1}					rotatory strengths, 10^{44} × esu^2 cm^2				absorption intensities, km/mol				
					LMO/	VCT/	VCT/					exptl	
calc[a]	calc[b]	calc[c]	calc[d]	exptl	6-31G*	6-31G*	6-31G*$^{(0.3)}$	exptl	6-31G*[e]	6-31G**	6-31G*$^{(0.3)}$	curv[f]	int[g]
1641	1477	1625	1462	1458	−0.1	7.3	5.2	−(weak)	0.2 (0.4)	0.1	0.4	7.9	
1640	1476	1624	1462		−6.1	−43.4	−30.0		8.3 (9.3)	8.4	8.5		
1633	1470	1617	1455	1444	5.8	−3.9	−2.7		4.1 (4.2)	4.9	4.8	11.8	
1629	1466	1613	1452		8.9	33.6	27.4		5.9 (5.6)	6.3	7.9		33.3
1592	1433	1568	1411	1394	36.5	57.0	60.7	58.1	4.6 (4.2)	4.6	6.2	4.7	
1566	1409	1528	1375	1376	−3.4	−4.4	−4.2		3.9 (4.4)	3.9	4.4	8.7	
1559	1403	1522	1370		19.2	66.7	31.6		5.1 (5.5)	4.1	3.7		
1462	1316	1434	1291	1295	−12.8	−37.6	−24.0	−4.3	6.0 (5.8)	5.4	5.5	2.5	1.8
1307	1176	1294	1165	1196	10.2	−6.9	6.9	5.4	4.4 (4.1)	4.5	3.7	0.8	
				(1165)[h]				12.8				(1.0)[h]	1.8
1290	1161	1273	1146	1154	21.9	59.0	35.4		6.0 (5.4)	5.2	3.2	0.6	
1233	1110	1210	1089	1088	−60.2	−125.4	−89.8	−38.7	19.8 (21.2)	19.4	16.3	4.4	
1189	1070	1172	1055	1057	−29.5	−84.1	−69.2	−30.1	14.5 (14.8)	14.7	17.0	7.2	17.3
1179	1061	1164	1048	1066	4.2	28.4	23.8		1.3 (1.3)	1.4	2.9	6.0	
1102	992	1083	974	989	−10.9	1.7	−1.7	−33.3	1.2 (1.6)	1.5	1.5	3.9	
1092	983	1079	971	978	−3.7	−28.3	−30.3		2.9 (2.9)	3.0	6.2	2.7	11.0
1066	959	1049	944	950	2.0	55.9	39.9	24.7	7.8 (7.1)	8.0	7.9	5.9	
900	810	887	798	834	16.1	48.8	29.8	28.0	1.7 (2.0)	1.7	1.6	weak	

[a] 6-31G*, unscaled. [b] 6-31G*, uniformly scaled by 0.9. [c] 6-31g*$^{(0.3)}$, unscaled. [d] 6-31G*$^{(0.3)}$, uniformly scaled by 0.9. [e] Numbers in parentheses are derived by the finite displacement method. [f] Curve fit to CCl_4 spectrum, Figure 3. [g] Integrated, Figure 3. [h] Overtone.

intensity calculation. However, since the numerical displacement procedure was used in the LMO–VCD calculation, the LMO absorption intensities are slightly different due to the numerical errors expected in the displacement calculations.

Recent studies by Rauk and Yang[21] have showed no significant improvements by use of electron-correlated excited-state wave functions in the summation in the expression for the magnetic dipole transition moment (eq 3). Magnetic dipole transition moments in the current VCT formulation are evaluated in the common origin (CO) gauge with origin at the molecular center of mass. The electronic ground state is approximated by the Hartree–Fock (SCF) determinantal wave function, and the excited states involved in the summation in eqs 2 and 3 are approximated as singlet-spin-adapted singly excited configurations derived from the Hartree–Fock wave function. Simulated IR and VCD spectra were obtained using frequencies scaled by 0.9 to bring them into closer agreement with experiment[41] and assuming a Lorentzian line shape of 5 cm^{-1} half-width at half-height.

Results and Discussion

The structure (*R,R*)-2,3-dimethylthiirane optimized at the RHF/6-31G*$^{(0.3)}$ level is shown in Figure 1, together with the structures of the (*R*)-2-methylthiirane and the parent thiirane. Details for the three molecules are listed in Table II. No experimental determinations of the geometries of the methyl and dimethyl derivatives have been reported. The calculated geometry of the parent thiirane is in excellent agreement with the experimental (microwave) geometry,[42] which is also given in Table II. In particular, the geometry of the ring is well reproduced with the 6-31G*$^{(0.3)}$ basis set, with which a more realistic C–C bond length is obtained.[43] The methyl substitution is predicted to have a negligible effect on the geometry of the ring.

The harmonic frequencies of the dimethylthiirane and its *2,3-d*$_2$ isotopomer calculated by the 6-31G* and 6-31G*$^{(0.3)}$ basis sets, together with observed frequencies, are listed in Table III. Calculated harmonic frequencies obtained by both basis sets are uniformly scaled by 0.9 in Tables IV–VI; this procedure brings the theoretical values into closer agreement with experiment (average rms deviations for the data presented in Tables IV–VI: 6-31G*, 20 cm^{-1}; 6-31G*$^{(0.3)}$, 13 cm^{-1}). Slight relative shifts are found in the calculated frequencies with the two basis sets, but

(41) Pople, J. A.; Schlegel, H. B.; Krishnan, R.; De Frees, D. J.; Binkley, J. S.; Frisch, M. J.; Whiteside, R. A.; Hout, R. F.; Hehre, W. J. *Int. J. Quantum Chem., Quantum Chem. Symp.* **1981**, *15*, 269.

(42) (a) Okiye, K.; Hirose, H.; Lister, D. G.; Sheridan, J. *Chem. Phys. Lett.* **1974**, *24*, 111–113. (b) Cunningham, G. L., Jr.; Boyd, A. W.; Meyers, R. J.; Gwinn, W. D.; Le Van, W. I. *J. Chem. Phys.* **1951**, *19*, 676–685.

(43) It was previously found[21] that the 6-31G*$^{(0.3)}$ geometry of oxirane is in substantially better agreement with experiment than the 6-31G* geometry.

Table V. Experimental and Theoretical Vibrational Properties for (*R,R*)-2,3-Dimethylthiirane-*2,3-d*$_2$ in the 1600–700-cm^{-1} Region

frequencies, cm^{-1}					rotatory strengths, 10^{44} × esu^2 cm^2				absorption intensities, km/mol			
					LMO/	VCT/	VCT/				exptl	
calc[a]	calc[b]	calc[c]	calc[d]	exptl	6-31G*	6-31G*	6-31G*$^{(0.3)}$	exptl	6-31G*[e]	6-31G*$^{(0.3)}$	curv[f]	int[g]
1639	1475	1623	1461	1452	6.7	28.6	19.6	−(weak)	2.4 (2.9)	2.5	10.0	27.2
1638	1474	1623	1461		−7.8	−46.7	−32.0		7.5 (8.4)	7.6		
1631	1468	1615	1453	1439	−1.7	−15.3	−12.7	7.6	1.4 (1.4)	1.9	9.0	
1629	1466	1612	1451		8.7	31.6	25.5		6.3 (6.1)	8.5		
1568	1411	1532	1379	1375	−2.5	5.5	0.5	−2.6	0.3 (0.5)	0.0	7.8	
1564	1408	1526	1373		−3.9	−7.3	−5.9		4.1 (4.7)	4.3		
				(1343)[h]							(1.1)[h]	
1491	1342	1478	1330	1323	23.8	45.1	37.1	20.7	3.7 (3.8)	5.3	2.1	
1268	1141	1250	1125	1129	−10.2	−31.7	−21.2	−19.9	5.6 (5.2)	7.5	3.7	23.6
1242	1118	1227	1104	1115	−4.5	−19.8	−13.8		0.5 (0.5)	0.5	0.5	
1191	1072	1175	1058	1065	−12.6	−52.0	−36.9	−32.9	5.8 (6.7)	4.6	1.5	
1184	1066	1167	1050	1053	−8.3	−8.8	−15.0		26.0 (26.4)	26.3	13.5	
1147	1032	1132	1019	1032	−4.2	−5.6	−1.7	−(weak)	4.1 (4.4)	6.6	4.2	
1009	908	995	896	913	11.4	15.7	6.6	12.1	0.5 (0.4)	0.2		0.3
917	825	902	812	835	0.6	−4.4	−9.0	weak	0.5 (0.6)	1.2		1.2
871	784	858	772	802	3.6	21.0	17.2	weak	0.4 (0.6)	0.6		
862	776	842	758	757	−13.2	50.2	40.3	weak	10.5 (10.0)	10.2		7.8
851	766	832	749	757	14.5	15.4	10.1		6.2 (5.6)	4.7		

[a] 6-31G*, unscaled. [b] 6-31G*, uniformly scaled by 0.9. [c] 6-31g*$^{(0.3)}$, unscaled. [d] 6-31G*$^{(0.3)}$, uniformly scaled by 0.9. [e] Numbers in parentheses are derived by the finite displacement method. [f] Curve fit to CCl_4 spectrum, Figure 3. [g] Integrated, Figure 3. [h] Overtone.

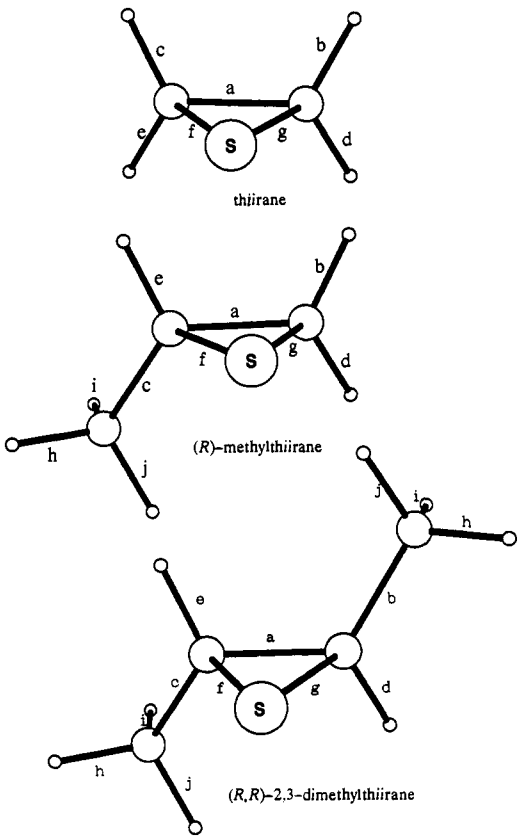

Figure 1. Structures of thiirane, (*R*)-2-methylthiirane, and (*R,R*)-2,3-dimethylthiirane. Refer to Table II for the parameter values.

the qualitative assignments are identical. Comparison of calculated IR and VCD intensities by the two methods and basis sets suggest a 1:1 correspondence between the calculated normal modes and those observed experimentally for all modes with the possible exception of one pair which has tentatively been reversed in Table III. The assignments are discussed further below.

The vibrational modes can be described by arbitrarily chosen internal coordinates, and such descriptions based on observation of the animated normal modes from 6-31G*$^{(0.3)}$/6-31G* calculations are also presented in Table III. An alternative approach to visualize the vibrational motions is to look at a static display of the three-dimensional atomic displacements. The ORTEP program[44] has been adapted for this purpose, and the resulting motions are displayed in Figure 2. The equilibrium geometry is displayed as open circles, and the displaced atoms are displayed as hatched circles. Each displaced atom is connected to its equilibrium position by a narrow line.

In the experimental region 1600–700 cm^{-1}, each methyl group is expected to have two antisymmetric bending modes, one symmetric bending mode, and two rocking modes. Thus 10 vibrational bands are expected to originate from the two methyl groups. This region is also expected to have one C*–C* stretching mode, two C*–C stretching modes, and four methine hydrogen (or deuterium) bending modes. The C*–S stretching, heavy-atom bending, and methyl torsions are expected to fall outside this region. Even though such group assignments are useful for discussion purposes, the normal vibrations are usually more delocalized, as can be seen in Figure 2. Therefore the concept of group assignments is approximate, and this should be remembered in relying on the assignments given in Table III.

The experimental IR and VCD spectra, in the 1500–700-cm^{-1} region, for (*R,R*)-2,3-dimethylthiirane and (*R,R*)-2,3-dimethylthiirane-*2,3-d*$_2$ in CCl_4 and CS_2 solutions are shown in Figure 3. Simulated IR and VCD spectra in the 1600–700-cm^{-1} range for the undeuterated dimethyl compound, calculated by LMO/6-31G*, VCT/6-31G*, and VCT/6-31G*$^{(0.3)}$, are shown in Figure 4. The computed data for the deuterated compound are similarly presented in Figure 5. Details for the d_0 and d_2 systems are listed in Tables IV and V, respectively. Although the frequencies and absorption intensities were also calculated with the 6-31G** basis set (see Tables III and IV), they are not emphasized here because of insignificant changes from the results obtained with the 6-31G* basis set. Data for (*R*)-2-methylthiirane are presented in Table VI and Figure 5.

(*R,R*)-2,3-Dimethylthiirane and (*R,R*)-2,3-Dimethylthiirane-*2,3-d*$_2$. The principal features of the IR and VCD spectra of the undeuterated (d_0) and deuterated (d_2) dimethylthiiranes are discussed below with reference to the data in Tables III–V and Figures 2–4. Frequencies mentioned are either experimental band positions or those calculated by the 6-31G*$^{(0.3)}$ ab initio force field and scaled by 0.9.

The positive CD band observed at 834 cm^{-1} in CS_2 (Figure 3) is well reproduced by both theoretical methods (Figure 4), which also correctly predict the IR intensity to be low. This band is due primarily to the stretch of the ring C–C bond mixed with the symmetric C*–CH_3 stretch. The band corresponds directly to the observed band in CS_2 solution at 802 cm^{-1} in the d_2 system

(44) Johnson, C. K. *ORTEP: A Fortran thermal-ellipsoid plot program for crystal structural illustrations*; Oak Ridge National Laboratory: Oak Ridge, TN, 1976.

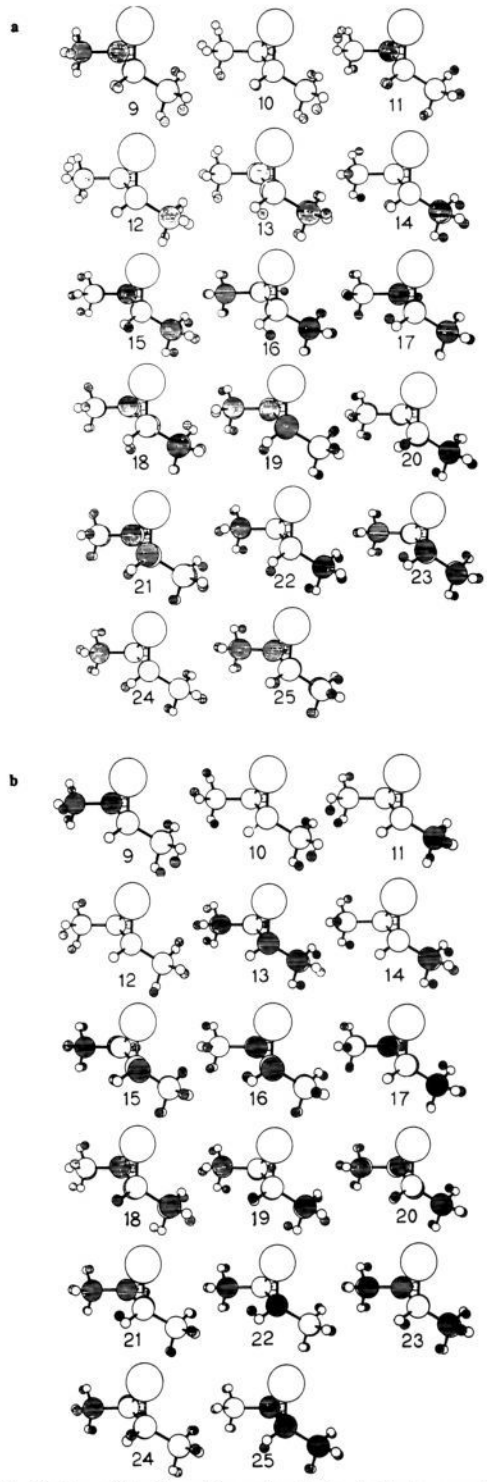

Figure 2. Display of the three-dimensional atomic displacements associated with the 6-31G* normal modes. The equilibrium geometry is displayed as open circles, and the displaced atoms, as hatched circles. Each displaced atom is connected to its equilibrium position by a narrow line. Wedged "bonds" connect atoms in the equilibrium structure: a, (*R*,*R*)-2,3-dimethylthiirane; b, (*R*,*R*)-2,3-dimethylthiirane-*2,3-d*$_2$. The vibrations are numbered in decreasing order of frequency. The first eight vibrations, corresponding to C–H or C–D stretching, are not shown.

(Figure 3) for which similar features are predicted (Figure 5) by VCT. The LMO method suggests that the 802-cm^{-1} band in the d_2 system should have a substantially weaker Cotton effect (CE), in better agreement with the CS_2 solution spectrum. The VCT method predicts substantially larger VCD than observed for this band.

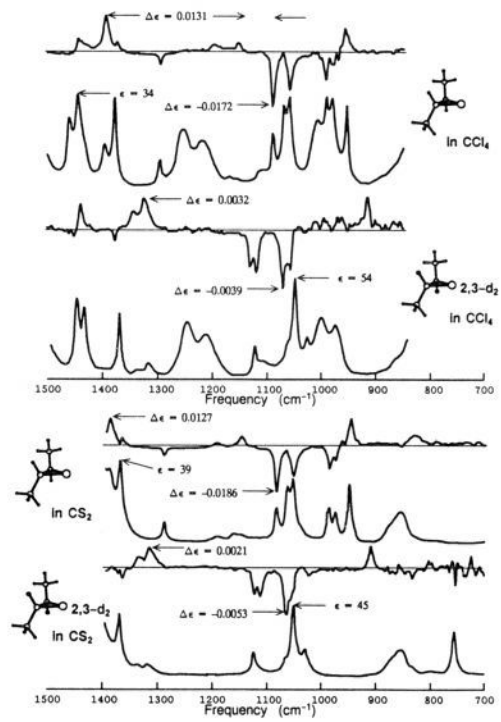

Figure 3. Vibrational absorption and circular dichroism spectra of (+)-*trans*-2,3-dimethylthiirane and of (+)-*trans*-2,3-dimethylthiirane-*2,3-d*$_2$ in CCl_4 solution and in CS_2 solution as labeled. The concentration and path length employed are 0.6 M and 490 μm for *trans*-2,3-dimethylthiirane and 0.5 M and 475 μm for *trans*-2,3-dimethylthiirane-*2,3-d*$_2$. All spectra are presented on arbitrary intensity scales. For quantitative data see Tables IV and V.

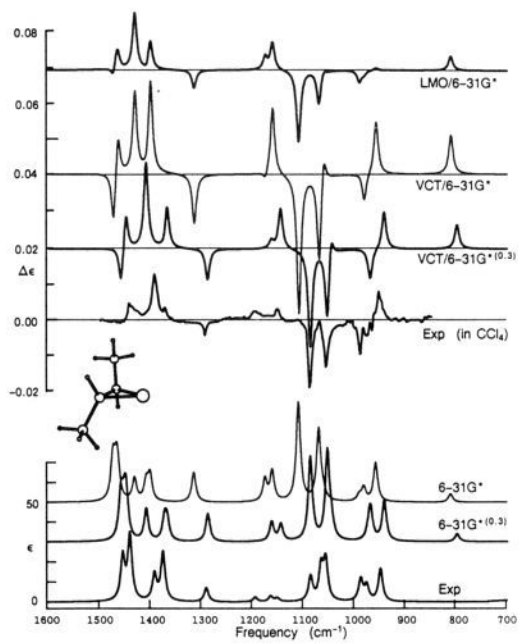

Figure 4. Simulated IR and VCD spectra for (*R*,*R*)-2,3-dimethylthiirane calculated by the LMO and VCT methods. The difference in the IR spectra is due to basis set. The ab initio frequencies have been scaled by 0.9. The experimental (CCl_4) IR spectrum is reproduced from the curve-fitted data of Table IV. The VCD scale applies to the theoretical spectra and also to the experimental VCD spectrum obtained in CCl_4 solution.

The moderately strong fundamental with a positive CE observed at 950 cm^{-1} is reproduced (Figure 4) quantitatively very well by VCT/6-31G*$^{(0.3)}$ but is predicted to be considerably weaker by

Table VI. Experimental and Theoretical Vibrational Properties for (*R*)-2-Methylthiirane

frequencies, cm^{-1}					rotatory strengths, $10^{44} \times esu^2\ cm^2$						absorption intensities, km/mol				
					LMO/	VCT/	VCT/	MFP/MP2[i]					MP2/	expt[j]	
calc[a]	calc[b]	calc[c]	calc[d]	expt[j]	6-31G*	6-31G*	6-31G*(0.3)	*f*	*g*	*h*	expt[j]	6-31G*[k]	6-31G*(0.3)	DZP	curv[l]	int[m]
1644	1480	1624	1462	1454	5.2	−0.6	−4.4	4.4	5.8	5.7	−0.6	4.1 (4.6)	4.9	3.5	4.9	
1640	1480	1617	1455	1443	1.0	−4.2	2.8	−5.1	−3.6	−5.5		6.3 (6.3)	3.9	7.9	4.0	
1628	1465	1603	1443	1434	5.3	13.3	9.1	3.1	4.3	5.0	6.0	3.6 (3.6)	6.9	4.5	5.6	22.9
1572	1415	1536	1382	1380	−1.9	−2.4	−0.4	2.9	2.7	0.9	weak	1.9 (1.9)	2.4	4.9	4.8	
1519	1367	1492	1343	1347	17.8	27.4	24.9	12.8	12.1	13.0	14.1	7.1 (7.5)	7.1	5.7	3.9	
1305	1174	1285	1156	1162	−7.8	−14.0	−7.6	5.8	3.3	3.0		3.3 (3.4)	2.1	3.2	1.5	
1285	1156	1273	1146	1158	15.9	20.0	17.3	3.2	−0.4	1.4	2.0	7.8 (8.3)	4.4	4.4	1.3	2.3
1223	1101	1195	1076	1070	−35.4	−75.0	−69.2	−20.2	−29.3	−34.9	−28.2[n]	26.7 (26.2)	22.6	24.3	10.4	
1183	1065	1150	1035	1038	0.7	13.5	12.0	1.7	1.3	5.9	6.4	7.2 (7.6)	8.4	5.5	5.2	18.6
1126	1013	1106	995	1001	4.2	40.4	27.9	14.2	28.92	26.5	19.4	2.6 (2.5)	2.8	4.2	2.7	
1032	929	1015	914	977	−12.7	−11.4	−10.4	−7.9	−8.5	−8.0	−10.3	2.2 (2.6)	2.7	1.9	3.4	
1010	909	990	891	966	9.6	10.1	7.7	−0.9	−1.6	−10.4		2.4 (2.4)	3.1	3.5	1.9	7.2
954	859	940	846	924	−5.0	−4.4	−7.3	−7.4	−0.8	−2.3	−8.7	1.6 (1.6)	1.8	2.6	2.0	

[a] 6-31G*, unscaled. [b] 6-31G*, uniformly scaled by 0.9. [c] 6-31g*(0.3), unscaled. [d] 6-31G*(0.3), uniformly scaled by 0.9. [e] MP2/DZP. [f] Distributed origin gauge. [g] Common origin at the center of the mass. [h] Common origin at the sulfur atom. [i] From ref 24. [j] From the spectra reported in ref 25. [k] Numbers in parentheses are derived by the finite displacement method. [l] Curve fit to CCl_4 spectrum. [m] Integrated. [n] This magnitude is uncertain due to the noise resulting from excessive absorbance.

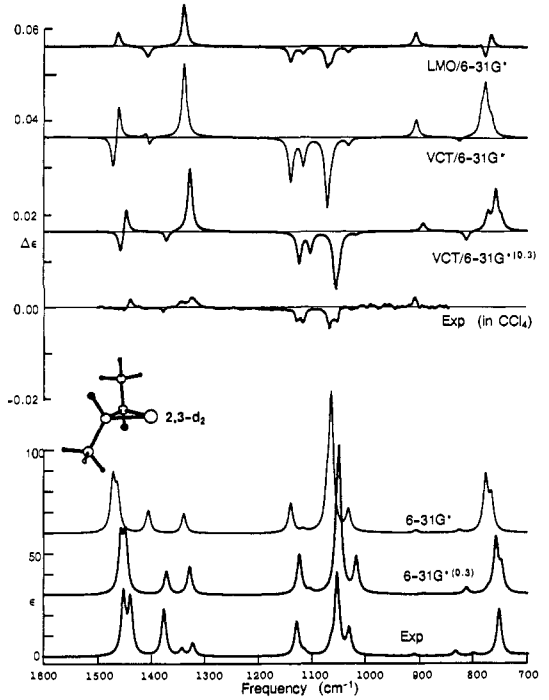

Figure 5. Stimulated IR and VCD spectra for (*R*,*R*)-2,3-dimethylthiirane-*2,3-d*$_2$ calculated by the LMO and VCT methods. The difference in the IR spectra is due to basis set. The ab initio frequencies have been scaled by 0.9. The experimental (CCl_4) IR spectrum is reproduced from the curve-fitted data of Table V. The VCD scale applies to the theoretical spectra and also to the experimental VCD spectrum obtained in CCl_4 solution.

LMO/6-31G*. This mode results from a methyl rocking contribution coupled with an out-of-phase C*–H wag. The strong IR absorption observed at 757 cm^{-1} (Figure 3) in the d_2 isotopomer originates from the two perpendicular C*–D modes: one is calculated (after scaling) to occur at 758 cm^{-1}; the second weaker fundamental corresponding to an in-phase C*–D wag is predicted to occur at 749 cm^{-1}. These two are not resolved in the experimental spectrum. Very weak CD is observed near 757 cm^{-1}. The appearance is correctly reproduced (Figure 5) by the LMO method (but not the VCT method) by predicting oppositely signed (and therefore cancelling) CEs for the nearly degenerate transitions.

The closest counterpart of the 749-cm^{-1} transition of the d_2 compound in the undeuterated system is the fundamental of a symmetry calculated to occur at 974 cm^{-1} and to be almost degenerate with another at 971 cm^{-1}. The 6-31G* force field yields these modes in the same order but with wider separation (992 and 983 cm^{-1}, respectively). Two well-separated bands are observed experimentally in this region, at 978 and 989 cm^{-1}, both with negative CEs, the higher frequency band having the more negative CE and somewhat larger absorbance. The LMO method predicts the correct signs and relative magnitudes of the CEs for these two bands whereas the VCT/6-31G*$^{(0.3)}$ method also predicts the correct signs but with the relative magnitudes reversed. The relative absorption intensities of these two bands have a 1.3:1 ratio in the experimental spectrum, but they have a 1:2 ratio in the 6-31G* (and 6-31H**) spectrum and a 1:4 ratio in the 6-31G*$^{(0.3)}$ spectrum. If we switch the order of the computed bands, the calculated absorption would be in the right order, with the 6-31G* basis set results better reflecting the experimentally observed relative intensities than the 6-31G*$^{(0.3)}$ basis. In that case, the LMO/6-31G* method would predict the wrong order of VCD magnitudes. The VCT/6-31G*$^{(0.3)}$ method would predict signs and order. It is not possible to judge conclusively whether or not the computed order of the bands is correct with the available data. For the present, it appears best to leave the order of the bands as predicted by both ab initio force fields.

The *appearance* of the experimental VCD spectrum of the undeuterated compound in the region 1050–1100 cm^{-1} is well

reproduced by both the LMO and VCT methods. Closer examination, however, suggests that the ab initio force field leads to the incorrect order of the normal modes calculated to occur at 1048 and 1055 cm^{-1} and observed at 1057 and 1066 cm^{-1}. These two bands have similar intensities in the experimental IR spectrum, and it is the lower frequency (1057 cm^{-1}) band which has a strong negative CE. The relative dipole strengths are not well reproduced by either basis set, but the combined absorption intensity predicted for these two bands is reasonably close to the experimental value. Similarly, the combined theoretical rotatory strengths are also in reasonable agreement, the VCT/6-31G*(0.3) results being so as a result of a greater degree of cancellation. However, both theoretical methods are in agreement that the higher frequency absorbance has the negative CE. The data in Tables III and IV are consistent with the reversed assignments.

The most intense feature in both the experimental and calculated VCD spectra of the d_0 compound (Figure 3) is the negative CE at 1088 cm^{-1} (exptl). Both it and the negative CE at 1057 cm^{-1} (discussed above) are assigned as combinations of methine wagging and methyl rocking motions. Both basis sets overestimate the absorption intensity for the 1088-cm^{-1} band by a factor of 4. The VCT/6-31G*(0.3) and LMO/6-31G* methods predict the rotatory strengths to be about 2.3 and 1.5 times as large as observed, respectively, suggesting that the magnitudes of the magnetic dipole transition moments[45] of this transition are accurately predicted by both methods.

In the 1000–1150-cm^{-1} region, the d_2 isotopomer has five experimental bands at 1032, 1053, 1065, 1115, and 1129 cm^{-1}, all of them exhibiting negative CD. The 1065- and 1115-cm^{-1} bands have weak absorption intensities and large dissymmetry factors. Both LMO/6-31G* and VCT/6-31G*(0.3) reproduce this pattern qualitatively well. A comparison of the absorption and VCD magnitudes for the 1053- and 1065-cm^{-1} bands, combined, suggests that the LMO/6-31G* method underestimates the magnitudes of the magnetic dipole transition moments,[45] which are more accurately calculated by VCT/6-31G*(0.3). The same conclusion emerges from the data for the 1129- and 1115-cm^{-1} bands.

The positive CEs at 1154 and 1196 cm^{-1} and the negative CE at 1293 cm^{-1} of the parent d_0 compound are correctly predicted by both theoretical VCD methods (the VCT/6-31G* combination predicts the wrong sign for the 1196-cm^{-1} band). The assignments are given in Table III. A comparison of the absorption and VCD magnitudes for the isolated band at 1295 cm^{-1} indicates that the magnetic dipole transition moment[45] is overestimated by VCT/6-31G*(0.3).

A total of seven vibrational modes of the d_0 compound are predicted to occur in the range 1350–1460 cm^{-1}, four of which are resolved in the experimental spectra. Two pairs of in- and out-of-phase methyl deformations are identified with observed absorbances at 1444 and 1458 cm^{-1}. The out-of-phase combinations are predicted by VCT to have appreciable CEs, positive and negative, respectively. The LMO method predicts lower intensities than those predicted by VCT for these bands. The two theoretical methods disagree on the signs expected for both in-phase (a symmetry) combinations. Overall, the simulated LMO/6-31G* VCD spectrum bears a closer resemblance to the experimental spectra than does the VCT/6-31G*(0.3) VCD spectrum. The same is true for the overall integrated rotational strength in this region. Both methods predict a strong positive CE for the a symmetry methine wag (C*–C*–H bend) mixed with some methyl deformation which is observed at 1394 cm^{-1} and calculated at 1411 cm^{-1}. The a and b methyl umbrella motions calculated to be separated by 5 cm^{-1} are observed as a single absorption at 1378 cm^{-1} experimentally. The IR intensities are calculated to be similar, and both methods predict that the a symmetry mode should have a strong positive CE.

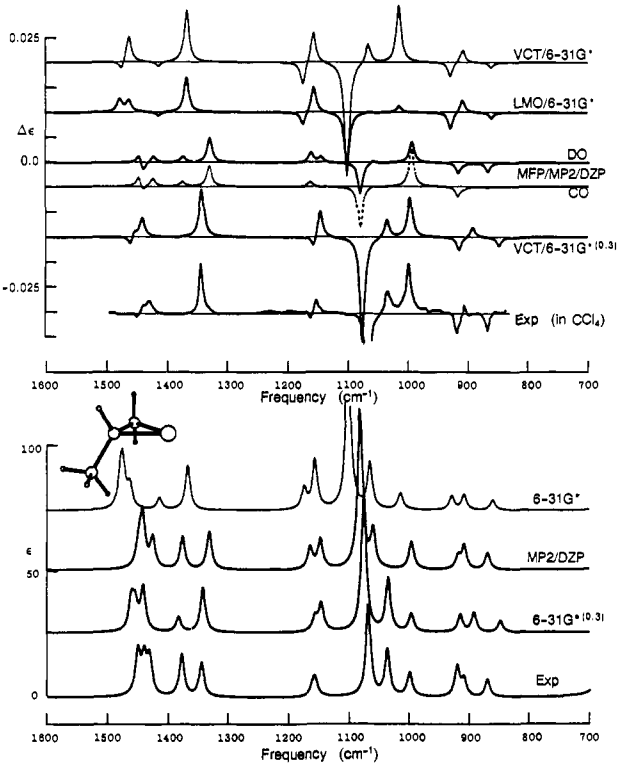

Figure 6. Simulated IR and VCD spectra for (*R*)-2-methylthiirane calculated by the LMO, VCT, and MFP methods (see text). The difference in the IR spectra is due to basis set and level of theory (RHF vs MP2). The ab initio frequencies have been scaled by 0.9 (RHF) or 0.94 (MP2). The experimental (CCl_4) IR spectrum is reproduced from the curve-fitted data of Table II. The VCD scale applies to the theoretical spectra and also to the experimental VCD spectrum obtained in CCl_4 solution.[25]

The corresponding region of the d_2 isotopomer spans the range 1323–1452 cm^{-1}. One of the five observed bands is assigned as an overtone (1343 cm^{-1}). Both force fields yield qualitatively correct band positions (after scaling), and both theoretical methods yield VCD results in very good agreement with the observed VCD spectrum. The weak negative CE at 1452 cm^{-1} is calculated to be the result of a near cancellation of a prominent negative CE due to the out-of-phase methyl deformation by the weaker positive CE due to the in-phase complementary motion. The VCT method overemphasizes this feature while it is underemphasized by the LMO method.

(*R*)-2-Methylthiirane. The previously published experimental VCD and IR spectra[25a] are shown in Figure 6, together with simulated VCT/6-31G* and VCT/6-31G*(0.3) spectra and previously published LMO/6-31G* spectra.[25a] In addition, MFP/DZP[24] VCD spectra in the DO and CO(center of mass) gauge have been reproduced from the published frequencies (scaled by 0.94) and intensities. All of the data for (*R*)-2-methylthiirane are listed in Table VI. Comparisons with the MFP/DZP results are of particular interest in that the force field and atomic polar tensors were derived from correlated (MP2) wave functions and it was claimed that use of the correlated ground-state wave function and force field was necessary to explain some features of the VCD spectrum in the mid-IR region.[24] In addition, comparison of the DO and CO(center of mass) MFP VCD intensities with the CO(center of mass) VCT values and the experimental data provides an independent assessment of the degree of origin dependence to be expected in the CO results and the absolute agreement with experiment of the two theoretical approaches in the mid-IR region of the spectrum.

From inspection of the simulated IR spectra of Figure 6, it is evident that the MP2 frequencies and relative intensities are superior to the SCF values in two regions of the spectrum: the separation between the bands observed at 911 and 922 cm^{-1} is

(45) Deductions regarding the relative magnitudes of the electric and magnetic dipole transition moments by comparison of the calculated dipole and rotatory strengths is strictly valid only for the a symmetry modes where the moments are collinear by symmetry. The comparison based on magnitudes is only approximately valid for the b symmetry modes or for asymmetric molecules, since the intermoment angle is basis set, force field, and origin dependent.

Table VII. Comparison of Experimental and Theoretical Dissymmetry Factors[a] for Substituted Thiiranes

(*R,R*)-2,3-dimethylthiirane				(*R,R*)-2,3-dimethylthiirane-2,3-d_2				(*R*)-2-methylthiirane				
freq, cm^{-1}	exptl	LMO/ 6-31G*	VCT/ 6-31G*(0.3)	freq, cm^{-1}	exptl	LMO/ 6-31G*	VCT/ 6-31G*(0.3)	freq, cm^{-1}	exptl	LMO/ 6-31G*	VCT/ 6-31G*(0.3)	MFP(DO)/ DZP
1458	weak	−1.0	−4.5	1452	weak	−0.2	−2.0	1454	−0.2	1.9	−1.5	1.9
1458				1452				1443	0.9	1.0	1.8	−0.2
1444	3.3	4.4	6.6	1439	1.2	1.5	2.0	1434				
1444				1439				1380	?	−1.6	−0.3	0.9
1394				1375	−0.1	−1.0	−1.7	1347	4.9	3.6	5.3	3.2
1376				1375				1162	0.8	0.9	1.9	1.5
1376				1323	13.0	9.4	9.3	1158				
1295	−2.2	−3.2	−6.3	1129	−5.3	−3.2	−5.4	1070	−2.9	−1.7	−3.3	−1.0
1196	8.1	3.2	2.4	1115				1038	1.3	0.1	1.6	0.0
1154	9.3[b]	5.2	14.0	1065	−2.3	−0.8	−2.0	1001	7.2	1.9	11.1	3.6
1088	−9.6	−3.5	−6.7	1053				922	−1.8	−0.6	−0.5	−1.6
1057	−2.4	−1.9	−2.7	1032	weak	−1.1	−0.3	911				
1066				913	37.0	29.0	33.0	870	−3.8	−3.0	−3.8	−2.0
989	−5.0	−3.6	−4.5	835	weak	0.9	−68.0					
978				802	weak	5.2	25.0					
950	4.0	0.3	5.3	757	weak	0.1	2.8					
834	?	7.2	17.0	757								

[a] Dissymmetry factor is given as $4R/D$, where R is rotational strength and D is dipole strength. The dipole strength in $esu^2\ cm^2$ is obtained from absorption intensities (km/mol) as $3.987 \times 10^{-37} A/\nu$; ν is the frequency in cm^{-1}. Unscaled frequencies were used for the theoretical predictions. For cases where several bands overlap, the average frequencies and intensity sums were used. Values in multiples of 10^{-4}. [b] Contribution from a nonfundamental band is present here.

accurately reproduced, as are the relative intensities of the two absorptions at 1347 and 1380 cm^{-1}. However, the relative intensities of the 911- and 922-cm^{-1} absorptions are incorrectly predicted by the MP2 calculation. Also, the spacing and relative intensities of the sequence of peaks between 1000 and 1100 cm^{-1} is more accurately described by both SCF force fields, and the closely spaced pair of bands at 1160 cm^{-1} (which are not resolved in the IR spectrum but are evident in the VCD spectrum) are best calculated by the 6-31G*(0.3) force field, as are the group of absorptions around 1450 cm^{-1}. The details of the MP2/DZP geometry (which should be similar to the SCF/6-31G*(0.3) geometry) were not provided, so it is not possible to speculate on the effect of the geometry itself on the calculated intensities.

The VCD results obtained by the MFP method contain three major discrepancies when compared to the experimental VCD data.[25] A bisignate VCD feature is clearly evident in the experimental spectra at ~1160 cm^{-1}. The negative component of this couplet was not emphasized in the previous interpretation[25b] due to the uncertainties in the assignments that resulted from the 6-31G basis set. The 6-31G* and 6-31G*(0.3) calculations both confirm the two bands at ~1160 cm^{-1} in the experimental spectra to be originating from fundamental modes, and the associated bisignate features are well reproduced by the LMO and VCT methods. None of the MFP calculations reproduce this bisignate VCD feature. The second discrepancy is associated with the VCD of the highest frequency experimental band at 1454 cm^{-1}. The small negative VCD observed for this band is not reproduced by the MFP method either at the MP2 or at the SCF (not included in Table VI or Figure 6) level using the DZP basis set, although the same method predicts[23] negative VCD for this band at the SCF level using the 6-31G* basis set. The VCD results of MFP/MP2/DZP would match the experimental spectrum if the calculated order of the modes at 1536 and 1543 cm^{-1} were reversed. The third discrepancy occurs for the experimental band at 911 cm^{-1}. While no significant VCD was observed for this band in CS_2 solution, a small positive VCD was apparent in CCl_4 solution. VCD associated with this band is best characterized as very weak. The MFP/MP2/DZP calculations with common origin gauge predict substantially large negative VCD for this band while the same calculations with distributed origin gauge predict small negative VCD. On the contrary, the LMO and VCT methods predict larger positive VCD.

The dissymmetry factors obtained from the recent VCD spectra[25a] are more accurate than those obtained from the earlier study[25b] because the earlier values were obtained from the peak intensities and the signal-to-noise ratio in those data was not as high as that in the recent data.[25a] A comparison of these dissymmetry factors (Table VII) indicates that the VCT/6-31G*(0.3) method provides a remarkably good agreement with the experimental data. Accordingly, the simulated spectra favor VCT/6-31G*(0.3), LMO, and MFP predictions, in that order.

Conclusions

A qualitative comparison of the theoretical spectra with the experimental spectra reveals that there is generally good agreement between the predicted and observed signs for the three thiiranes considered here. This indicates that the ab initio VCD methods can be confidently used to determine the absolute configuration when the experimental VCD spectrum is known for a molecule with unknown configuration.

To evaluate the consequences of approximations involved in each of the three different theoretical methods, a quantitative comparison with the experimental data is essential but is soured by the ever-present specter of basis set deficiencies. Nevertheless, the absolute performance of the methods employed in the present study may be assessed by comparison with experimental data in Tables IV–VII. In the LMO method,[7-9] orbital-rocking contributions to the total magnetic dipole transition moment are estimated to be small and are ignored. This estimate appears reasonable as deduced from recent paramagnetic magnetizability calculations.[46] From the quantitative comparisons of LMO/6-31G* VCD predictions with the corresponding observed values, it appears that the LMO method underestimates the magnetic dipole transition moments[45] in most cases. On the other hand, the VCT/6-31G*(0.3) method tends to overestimate the magnetic dipole transition moments for the methylthiiranes. The opposite was found to be true in the case of the methyloxiranes.[21] For the dimethylthiiranes considered here, no clear advantage of one method over the other emerges except for the 700–800-cm^{-1} region, where the LMO method provides more accurate predictions. For the methylthiirane, the VCT/6-31G*(0.3) method yields better results.

The principal approximation in the present implementation of VCT, which distinguishes it from the otherwise formally equivalent (at the SCF level) MFP method, is the lack of electron correlation in the sum over excited states which is involved in the expression for the magnetic dipole transition moment. For as yet unexplained reasons, the MFP method at the SCF level is not as successful at reproducing the experimental VCD spectrum of methylthiirane.[23] Substantial improvement is achieved by use of the MP2 force field and electric dipole transition moments,[24] although some

(46) (a) Polavarapu, P. L. *Chem. Phys. Lett.* **1990**, *171*, 271–276. (b) Polavarapu, P. L. *Chem. Phys. Lett.* **1991**, *179*, 9–12.

notable discrepancies are still present. It would be of interest to compare MFP results for the dimethylthiiranes.

Acknowledgment. The financial support of the NIH (Grant GM29375), the NSF (Grant CHE8808018), and the Natural Sciences and Engineering Research Council of Canada is gratefully acknowledged. We also thank the Supercomputer Services of the University of Calgary for generous allocations of CPU time on the CDC Cyber 205 computer.

Registry No. (2*R*,3*R*)-2,3-Dimethylthiirane, 70095-46-4; (2*R*,3*R*)-2,3-dimethylthiirane-2,3-d_2, 136749-28-5; (*R*)-2-methylthiirane, 17406-93-8; (2*S*,3*S*)-2,3-dimethylthiirane-2,3-d_2, 136781-46-9; (*S*)-2-methylthiirane, 136749-29-6.

The Cope Rearrangement Revisited

Michel Dupuis,*,† Christopher Murray,‡ and Ernest R. Davidson‡

Contribution from IBM Corporation, Department 48B/MS 428, Neighborhood Road, Kingston, New York 12401, and Department of Chemistry, Indiana University, Bloomington, Indiana 47405.
Received May 13, 1991

Abstract: Using a CASSCF wave function and a 6-31G* basis set we have located several stationary points on the potential energy surface for the Cope rearrangement. At this level of theory we find both a synchronous path through a symmetrical aromatic transition state and a non-concerted path through a disymmetrical transition state followed by a symmetrical biradicaloid intermediate. After zero-point and thermal corrections both paths appear possible. A more elaborate description of electron correlation does not yield a clear preference for either path.

I. Introduction

Synchronicity and concertedness in the vicinity of the transition states in the Cope rearrangement, and the structure of these transition states, continue to be the subject of intense debate. A review of the present state of knowledge on this problem has recently been published.[1] In this discussion we will follow Dewar's definition that "concerted" implies a one-step mechanism with no stable intermediate while "non-concerted" implies a multiple-barrier reaction path with at least one stable intermediate. Unfortunately, for a nearly flat potential energy surface a calculated reaction mechanism can change between concerted and non-concerted as the quality of the theory is changed. For a concerted path Dewar defines "synchronous" as one where all bonding changes have taken place to a more-or-less equal extent and "non-synchronous" as one where some changes are much more complete than others. "Synchronicity" is only loosely defined. It is unclear what CC bond length would correspond to a "half-broken" bond. Also, at a symmetrical transition state, the reaction coordinate (the normal mode of imaginary frequency) will necessarily make equal and opposite changes in the equivalent forming and breaking bonds so all concerted reactions with identical reactants and products will be locally synchronous.

For the Cope rearrangement, the C_3–C_4 bond length and the number of imaginary frequencies at the midpoint of the reaction are indications of concertedness and synchronicity. This interallylic CC bond length in the chair and boat conformations of the transition-state region is also the key parameter which reflects the biradical or aromatic character of the structures involved in the rearrangement. Additionally, orbital occupation numbers are sometimes discussed.

Some recent attempts to resolve the discrepancy between semiempirical[2,3] and ab initio studies[4-7] have used perturbation and configuration interaction methods based on self-consistent-field (SCF) orbitals. The sensitivity of the optimized structures to the level of theory used[4] suggests that the bias introduced by using SCF orbitals is very difficult to overcome. This is of paramount importance, of course, since the key issue in this problem is the amount of biradical character in the transition structures.

In this respect the ab initio study by Dewar and Healy[6] is seriously flawed. They attempted to use closed-shell SCF followed by MPn to calculate the relative energy of the aromatic and biradicaloid structures. But for true biradicaloids, like H_2 at large internuclear distances, this procedure fails. A more correct, but still dubious, procedure is to use UHF with a broken symmetry wave function followed by UMPn. It is no wonder that Dewar was unable to find a biradicaloid structure with a RHF wave function.

In this paper, we report calculations which follow the more desirable approach of Osamura et al.[4] and Morokuma et al. (MBH).[5] They are based on a multiconfiguration SCF (MCSCF) form of the wave function which has enough flexibility to take into account the most significant electron correlation effects associated with bond breaking and bond formation in the rearrangement. However, the present study goes beyond the work of these researchers in the use of a polarized basis set throughout. As will become clear later, this larger basis set yields significantly different relative energies, compared to the results of MBH. Seven stationary points on the potential energy surface have been characterized, including three genuine transition states and two stable intermediates with comparable energies. The role of these species in the rearrangement has been investigated by characterizing the intrinsic reaction coordinate (IRC). One of the two stable intermediate structures determined in this work has not been characterized previously, to the best of our knowledge. Also, one of the transition states has not been found before in ab initio calculations.

II. Overview of Results

A total of seven stationary points on the potential surface were characterized with MCSCF (6-31G*) wave functions and are depicted in Figure 1. They are the following: (1) the allyl + allyl structure, whose energy is used as a reference; (2) a loose boat transition state with an interallylic distance R = 2.615 Å,

† IBM Corporation.
‡ Indiana University.

(1) Borden, W. T.; Loncharich, R. J.; Houk, K. N. *Annu. Rev. Phys. Chem.* **1988**, *39*, 213.
(2) Dewar, M. J. S.; Jie, C. *J. Am. Chem. Soc.* **1987**, *109*, 5893.
(3) Dewar, M. J. S.; Jie, C. *J. Chem. Soc., Chem. Commun.* **1987**, 1451.
(4) Osamura, Y.; Kato, S.; Morokuma, K.; Feller, D.; Davidson, E. R.; Borden, W. T. *J. Am. Chem. Soc.* **1984**, *106*, 3362.
(5) Morokuma, K.; Borden, W. T.; Hrovat, D. A. *J. Am. Chem Soc.* **1988**, *110*, 4474.
(6) Dewar, M. J. S.; Healy, E. F. *Chem. Phys. Lett.* **1987**, *141*, 521.
(7) Hrovat, D. A.; Borden, W. T.; Vance, R. L.; Rondan, N. G.; Houk, K. N.; Morokuma, K. *J. Am. Chem. Soc.* **1990**, *112*, 2018.

0002-7863/91/1513-9756$02.50/0